applied sciences

MDPI

Article

Experimental and Numerical Study on the Effect of Three-Hole Simultaneous Blasting Technology on Open-Pit Mine Bench Blasting

Xiaojun Zhang [1,2,*], Zhuo Li [2,*], Zheng Wei [3] and Wenxue Gao [2]

[1] Hubei Key Laboratory of Blasting Engineering of Jianghan University, Wuhan 430056, China
[2] Faculty of Architecture, Civil and Transportation Engineering, Beijing University of Technology, Beijing 100124, China
[3] Inner Mongolia Kinergy Blasting Co., Ltd., Ordos 017000, China
* Correspondence: zhangxj@bjut.edu.cn (X.Z.); lz1074628512@163.com (Z.L.)

Abstract: Blasting technology is widely applied in various engineering applications due to its cost-effectiveness and high efficiency, such as in mining, transport infrastructure construction, and building demolition. However, the occurrence of cracking in the rear row has always been a major problem that disrupts mining bench blasting. To address this issue, a three-hole simultaneous blasting technology is proposed in this study. Both numerical simulations and onsite blasting experimental testing were conducted. To aid this endeavor, the three-hole simultaneous blasting and the hole-by-hole blasting methods were adopted to comparatively analyze the severity of the damage caused to the original rock and the effect of rock fragmentation in the rear row. The obtained results highlighted that the outcome of the blast produced by the three-hole simultaneous blasting method is satisfactory, with fewer flying stones and concentrated blasting piles required. Additionally, the original rock in the rear row showed no obvious sign of tensile damage and had uniform fragmentation. It was also found that a block size of less than 60 cm accounts for 100%, while a block size of less than 50 cm accounts for 98.7% of the whole blocks, with no large blocks reported. Moreover, a penetrating horizontal crack occurred in the direction of the connection of the blast hole center when the three-hole simultaneous blasting method was adopted. This resulted in a smooth and flat rear part of the rocks at the interface. Compared to the hole-by-hole blasting method, the three-hole simultaneous blasting method improved the effective stress and displacement at each measurement point. At the measurement point directly at the front of the borehole, the maximum effective stress attained 67.9 GPa, and the maximum displacement reported was 31.9 cm. Overall, it was shown that the three-hole simultaneous blasting technology is applicable in similar applications of mine bench blasting, which is conducive to addressing the rear row original rock strain for onsite bench blasting.

Keywords: bench blasting; three-hole simultaneous blasting; digital electronic detonator; hole-by-hole blasting; numerical simulation

check for updates

Citation: Zhang, X.; Li, Z.; Wei, Z.; Gao, W. Experimental and Numerical Study on the Effect of Three-Hole Simultaneous Blasting Technology on Open-Pit Mine Bench Blasting. *Appl. Sci.* **2024**, *14*, 2169. https://doi.org/10.3390/app14052169

Academic Editor: Ricardo Castedo

Received: 17 November 2023
Revised: 30 January 2024
Accepted: 30 January 2024
Published: 5 March 2024

Copyright: © 2024 by the authors. Licensee MDPI, Basel, Switzerland. This article is an open access article distributed under the terms and conditions of the Creative Commons Attribution (CC BY) license (https://creativecommons.org/licenses/by/4.0/).

1. Introduction

Due to its relatively low cost and high efficiency [1,2], blasting technology is widely adopted in various engineering applications across a wide range of domains, such as mining, transport infrastructure construction, and building demolition [3–5]. In recent years, a large number of new blasting equipment has entered the blasting industry, among which the digital electronic detonator has been highly recognized by many researchers and users due to its simple operation, high delay accuracy, and detectable blasting network [6,7].

In order to investigate the influence of delay time on rock fragmentation, Tang et al. [8] conducted eight experiments employing bench blasting models with double holes. The results reported a significant difference and great improvement in fragmentation when the delay times were in the range of a no shock wave interaction compared to other interactions.

When determining the optimum delay time in multihole blasting, except for the stress wave interaction, key factors such as crack propagation should be considered. Zhang et al. [9] examined the open-cut bench blasting at the Barun Eboxi Mine of the Baotou Iron and Steel Group by conducting a theoretical analysis of the shock wave, performing numerical simulations, and carrying out field tests. The study found that under the condition of a 24 m high bench, the use of intermediate air intervals is beneficial to rock fragmentation. In another work, Hosseini et al. [10] examined the effect of several blasting parameters on bench blasting. A total of 32 experiments have been designed and conducted, and numerical simulations were also carried out using the LS DYNA (R14.0) software to evaluate the blast results. As a result, it was reported that the blast hole diameter is the most important factor influencing blasting outcomes. Dzimunya et al. [11] used the random forest algorithm to develop a model for predicting the blast-induced ground vibrations from bench blasting using 48 dataset records. The model was trained and tested by employing the WEKA data-mining software (3.9.5). The study results demonstrated that the random forest model can effectively predict the peak particle velocity (PPV). Additionally, it was noted that the equivalent-path-based equation is a suitable empirical method for predicting the PPV. In their study, Lv et al. [12] used digital electronic detonators in large-scale iron ore mining. The implementation not only improved the outcome of blasting but also reduced the damage caused by blasting vibrations. As a result, a higher shovel efficiency was reported. In a connected study, Cheng et al. [13] used a digital electronic detonator for the excavation of high-side slopes. It was shown that this approach is effective in reducing blasting vibrations and high block rates and lowering the workload of secondary crushing. Also, He et al. [14] applied the digital electronic detonator to achieve large-scale delayed blasting using reasonable blasting parameters and an explosion network. The application yielded a satisfactory blasting outcome. Chen et al. [15] calculated the blast hole charge amount based on a three-dimensional solid model of the blasting rock mass, aiming to make full use of drilling data and improve the blasting efficiency. Considering the application example of No. 918 Bench Blasting of the Shengli Open-pit Coal Mine in Xilinhot, Inner Mongolia, the blast hole charge amount in the blasting area was calculated and compared against the results of a single hole rock property calculation. The results showed that the blast hole charge calculated by the three-dimensional rock mass model can be effectively reduced. In their study, Hosseini et al. [16] focused on predicting the PPV in surface mines using machine learning ensemble technologies. The results indicated that ensemble models are capable of increasing the accuracy of the PPV predictions in comparison to the most accurate individual models. However, the sensitivity analysis carried out indicated that the spacing ($r = 0.917$) and the number of blast holes ($r = 0.839$) had the highest and lowest impacts on the PPV intensity, respectively.

Nevertheless, in onsite practice and applications, it is often reported that the outcome of bench blasting in the last row of holes is unsatisfactory. Also, there is even a risk of rear row cracking or protrusions in some cases. To address this, a three-hole simultaneous blasting technology is proposed in this study by adopting the principle of stepwise blasting and the theory of smooth blasting in combination. By means of numerical simulations, a comparative analysis is conducted on the severity of damage caused by three-hole simultaneous blasting and hole-by-hole blasting. Finally, the rationality of the three-hole simultaneous blasting technology is verified using data from onsite experiments.

2. Three-Hole Simultaneous Blasting Technology

2.1. Principle of the Three-Hole Simultaneous Blasting

Based on the hole-by-hole blasting, three adjacent holes in the same row were combined into one group to accommodate the current engineering practice. The blast holes within the same group were simultaneously detonated, and the detonation was performed with a millisecond delay between different groups. This is referred to as the three-hole simultaneous blasting, as shown in Figure 1.

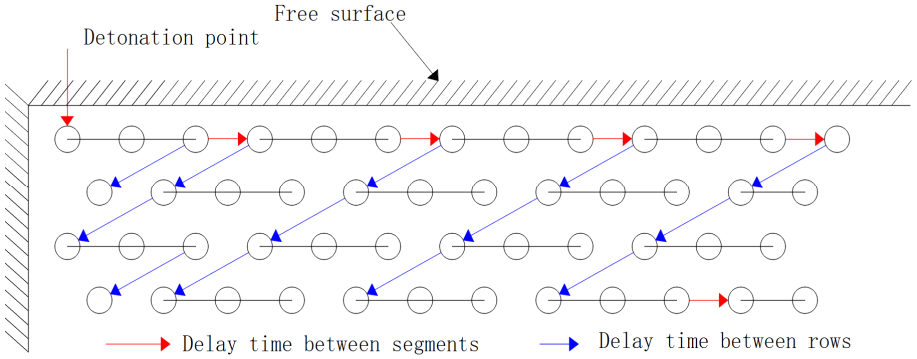


Figure 1. Schematic diagram of the three-hole simultaneous blasting.

As shown in the figure, three blast holes were combined into one section. The first blast hole tilted towards the free surface, separating the rock around the blast hole from the original rock. In addition, the first blast hole provided a free surface for the subsequent blasting of the other holes. This improved the outcome of the rock mass fragmentation. Before the disappearance of the stress field generated by the blasting of the first set of blast holes in the rock mass, the second set of blast holes was immediately detonated. In this regard, the stress waves created by the two sets of blast holes overlapped. This overlapping enhanced the stress waves, extended their effects, and improved the crushing effect. At the same time, the three holes formed a section in the last row of blast holes for bench blasting, which is similar to "smooth blasting". As a result, a neat fracture surface developed between the blast holes, reducing the vibration induced by blasting. This prevented the blast holes in the rear row from overturning or backlashing, in addition to facilitating shovel loading, excavation, and subsequent blasting.

2.2. Characteristics of the Three-Hole Simultaneous Blasting Technology

In general, the three-hole simultaneous blasting technology has the following advantages:

(1) Increasing the energy of rock mass interaction

The three-hole simultaneous blasting technology was applied to detonate three blast holes simultaneously. In this process, the amount of explosives used in one section is three times that required for hole-by-hole blasting. This increased the blasting energy in the same section while improving the outcome of the rock mass fragmentation. Compared to hole-by-hole blasting, the vibration induced by blasting fell within a controllable range [17,18].

(2) Reducing the ratio of large blocks

As mentioned above, the three holes within the same section were detonated simultaneously. In this case, the distribution of charge was relatively extensive, and the explosive load borne by the rock mass was relatively uniform [2,19]. This enabled sufficient fragmentation of the rock mass. After the detonation of the previous blast hole, a new free surface developed for the blasting of the subsequent blast hole. The free surface became more abundant, reducing the rate of large blasting blocks.

(3) Reducing the susceptibility of rear-hole blasting to overturning and backlashing

Considering the bench blasting, the large resistance line of the rear hole chassis caused a significant clamping effect and insufficient blasting energy. This phenomenon hindered the rock mass from moving horizontally. As a result, the rock mass tended to overturn or recoil in the rear holes [20]. On this basis, combining three holes into one can increase the blasting energy in the rear holes. Furthermore, detonating the three holes at the same time was beneficial to the formation of a neat fracture surface in the rear holes, thereby avoiding the risk of upward blasting and backlash in the rear holes.

3. Onsite Bench Blasting Test of Three-Hole Simultaneous Blasting

3.1. Case Study

In this section, the considered experimental testing site is described. The Xinguang Open-pit Mine is located in the middle east part of the Baiyun Wusu I exploration area, which falls within the jurisdiction of Qipanjing Town, Otog Banner, Ordos. Depending on the degree of geological exposure and borehole exposure, the order of strata from old to new is as follows: the Taiyuan Formation of the Upper Carboniferous System (C2t), the Shanxi Formation of the Lower Permian System (P1s), the Lower Shihezi Formation (P1x), and the Quaternary System (Q).

In terms of structure, the minefield is a monocline that inclines to the southwest, with a dip angle of 5~10° along the coal seam. The blasting area, considered a case study in this investigation, is shown in Figure 2.



Figure 2. The blasting area considered in this study.

3.2. Blasting Plan and Parameter Design

Due to the favorable environment in the surrounding areas, which is dominated by sandstone, a digital electronic detonator was employed in the design of tests in this work, with a precise delay and a three-hole simultaneous blasting scheme.

The main parameters of the open-pit deep hole bench blasting included the aperture, hole depth, ultra depth, chassis resistance line, hole spacing, row spacing, packing length, and explosive consumption per unit [21].

(1) Aperture d.

The aperture of the open-pit deep hole blasting is largely related to the type of drilling rig. In the blasting area considered in this study, the aperture was 90 mm.

(2) Hole depth L and super depth h

The depth of the hole is determined by the height and super depth of the step. In this blasting area, the 1270 flat plate step height was 12 m, with a vertical drilling rig operation.

Additionally, the ultra depth value is affected by the properties and structure of the rock mass, exhibiting a certain degree of proportionality with the diameter of the blast hole, as shown in Equation (1).

$$h = (5 \sim 10)d \tag{1}$$

By Equation (1), the calculated super depth was 450~900 mm. In this blasting area, the super depth was set to 0.8 m. As a result, the depth of the hole was given by:

$$L = H + h \tag{2}$$

By Equation (2), the depth of the hole was 12.8 m.

(3) Chassis resistance line W_1

The chassis resistance line was calculated considering the safety conditions of drilling operations as follows:

$$W_1 \geq H \cot \alpha + B \tag{3}$$

where W_1: Toe burden, in m;

α: The slope angle of the step, generally between 70° and 85°. In this design, it was taken as $\alpha = 80^{\circ}$;

H: Step height, in m;

B: The safe distance from the center of the borehole to the top line of the slope. In this design, it was taken as $B = 1.0$ m.

By calculation:

$$W_1 \geq 3.1 \text{ m} \tag{4}$$

In this design, the toe burden was considered as $W_1 = 3$ m.

(4) Hole spacing a and row spacing b

The hole spacing a was calculated using Equation (5).

$$a = mW_1 \tag{5}$$

where m represents the density coefficient of the blast holes. In this design, m was taken as $m = 1.2$. As a result, the hole spacing was given as:

$$a = 3.6 \text{ m} \tag{6}$$

In this design, the hole spacing was taken as $a = 4$ m.

When an equilateral triangle (Quincunx) is used to characterize the hole layout, the relationship between the row spacing and hole spacing was expressed as:

$$b = a \sin 60^{\circ} \tag{7}$$

By calculation, the row spacing was 3.46 m. In the present design, the hole spacing was taken as $b = 3$ m.

(5) Filling length l_2

The filling length l_2 was determined by Equation (8).

$$l_2 = (0.7 \sim 1.0)W_1 \tag{8}$$

By calculation, the filling length was 2.1 m~3.0 m. In this design, the filling length was taken as $l_2 = 3.0$ m.

(6) Unit explosive consumption q

Based on the rock solidity coefficient (f = 4~6) of sandstone in the blasting area, the sand shale (f = 3~5), and the prior experience in blasting, the unit explosive consumption was given by:

$$q = 0.4 \text{ kg/m}^3 \tag{9}$$

(7) Charge per hole Q

The charge per hole for the first row of holes was calculated using Equation (10).

$$Q = qaW_1H \tag{10}$$

where q: Unit explosive consumption, in kg/m^3;

a: Hole spacing, in m;

H: Step height, in m;

W_1: Toe burden, in m.

On this basis, the charge per hole in the first row was calculated as: $Q = 57.6$ kg. In the present design, it was taken as $Q = 60$ kg.

Starting from the second row of holes, the charge per hole for each subsequent row of holes was calculated using Equation (11).

$$Q = kqabH \tag{11}$$

where k denotes the increasing coefficient, which takes into account the effect of ore and rock resistance from the previous rows of holes, and $k = 1.1 \sim 1.2$. In this design, k was set to 1.1. b is the row spacing, in m.

From the second row of holes, the charge per hole was calculated with Equation (11). By calculation, the charge per hole was 63.36 kg. In this design, it was taken as $Q = 60$ kg.

3.3. Design of the Detonation Network

In this study, three adjacent holes along the same row were taken as one segment. The delay between adjacent sections within the same row was 25 ms, while that between different rows was 65 ms. Figure 3 presents a schematic diagram of the detonation network.

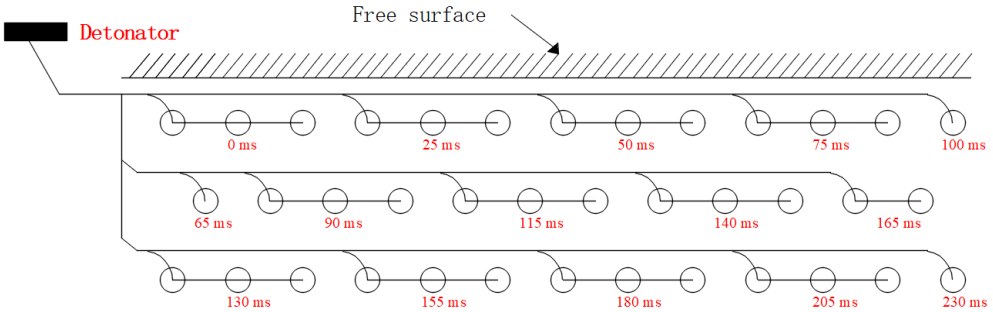


Figure 3. Schematic diagram of the detonation network.

3.4. Analysis of the Blasting Outcome

(1) Shape of the blasting pile

Before the detonation network was detonated, all operators were evacuated from the site. Overall, it was found that there were no rocks blasted too far away after detonation, and the blasting piles were relatively concentrated and of uniform size. Figure 4 shows the blasting piles with their corresponding shapes.

(2) Blasting outcome for the rear row rock mass



Figure 4. Shapes of the blasting piles.

After detonation, a waiting period was set for 15 min. When the smoke was fully gone, the blasting technician entered the blasting area to check the outcome of the blasting. It was found that strain barely occurred in the rear row. In this case, the outcome of separation

from the original rock was reported to be excellent, with a relatively smooth interface observed, as shown in Figure 5.

(3) Blasting block size

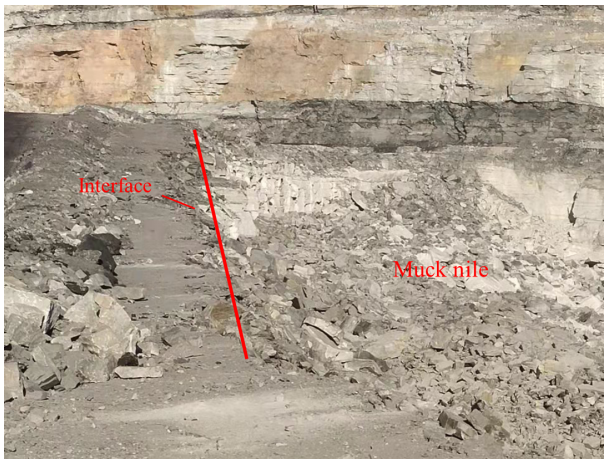


Figure 5. Blasting outcome in the rear row.

In the engineering applications of rock mass blasting, fragmentation was considered the most effective measure of the blasting-induced fragmentation outcome. In this experiment, the digital image fragmentation analysis software as Split-Desktop 4.0 was used to analyze the images of the blasting pile [22]. In this regard, the images of the pile should be taken immediately after the explosion. A standard-sized sphere was used as a reference for capturing the images. During the analysis process, it was necessary to set all relevant parameters. Additionally, non-rock block areas were covered with color blocks in the figure, and the position of the sphere was marked with color blocks. The size of a standard-sized sphere was inputted. Subsequently, the software can automatically analyze the blasting block size in the figures, obtaining the distribution of the blasting block size under experimental conditions [23]. Figure 6 presents a selected shooting image of the explosive pile in a certain area, with the red spherical object considered as a reference.

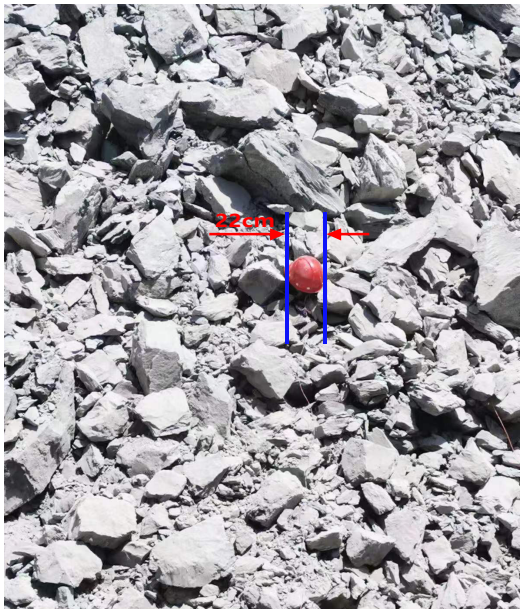


Figure 6. An image of the explosive pile in a certain area.

Then, the image to be processed was introduced into the Split-Desktop 4.0 software. With the size of the reference object marked, an appropriate density of division was set. The initial size and step size were set manually. Figure 7 shows the diagram of initial processing in the Split-Desktop 4.0 software.

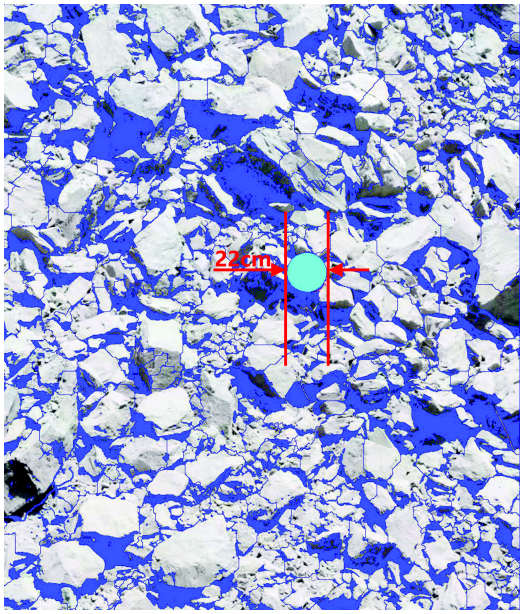


Figure 7. Initial processing diagram from Split-Desktop 4.0 software.

Table 1 lists the data obtained from the image processing using the Split Desktop 4.0 software. The data in the table were further processed, and a curve graph was generated, as shown in Figure 8.

Table 1. Degree distribution data of the crushed blocks.

Size (cm)	0.5	1.0	5	10	15	20	25	30	35	40	45	50	55	60
Passing (%)	1.6	3.2	14.9	29.0	42.5	56.2	69.5	80.2	88.1	93.4	96.9	98.7	99.6	100

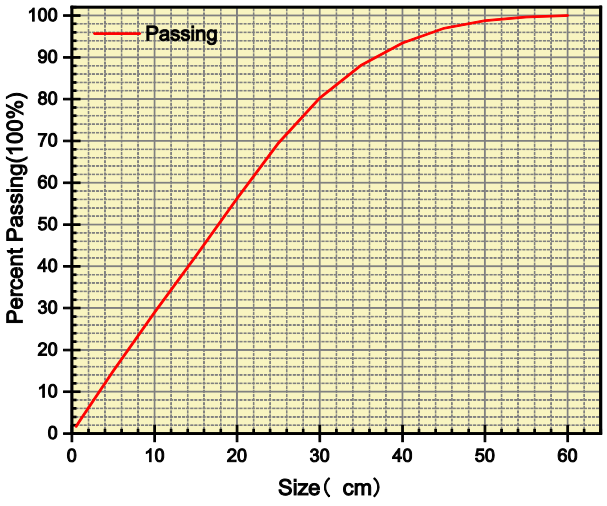


Figure 8. Degree distribution of the blasting blocks.

According to the practical experience gained from blasting engineering applications, a rock block with a size of over 65 cm was classified as a large-sized block. As shown in Table 1 and Figure 8, all the blocks had a size of less than 60 cm, and 98.7% of the blocks had a size of less than 50 cm. There was no generation of large blocks. Therefore, the onsite outcome of blasting in this study was deemed satisfactory.

4. Numerical Simulation Analysis of the Hole-by-Hole Blasting and Three-Hole Simultaneous Blasting

To further evaluate and analyze the effectiveness of the three-hole simultaneous blasting technology, a step blasting model was established employing the ANSYS/LS-DYNA (R14.0) numerical simulation software [24,25]. The evolution range and severity of rock damage in the rear row were comparatively analyzed considering the three-hole simultaneous blasting and the hole-by-hole blasting cases. By selecting the units at typical locations in the model and analyzing the effective stress and the changes in displacement in the observation point units, the characteristics of the hole-by-hole blasting and the three-hole simultaneous blasting methods were determined and evaluated.

4.1. Methodology for Numerical Simulation

4.1.1. Numerical Integration Procedure

Numerical studies of the hole-by-hole blasting and three-hole simultaneous blasting were carried out using the finite element method (FEM) with an explicit integration procedure. Massively parallel processing (MPP) LS-Dyna code, which uses explicit central difference time integration, was adopted. The dynamic equation solved during the calculations had the following form [26]:

$$M\ddot{x}_n = F_n^{ext} - F_n^{\text{int}} - C\dot{x}_n \tag{12}$$

where M is the diagonal mass matrix; F_n^{ext} is the external and body forces; F_n^{int} is the stress divergence vector; C is the damping matrix; and x, $\dot{x}$, $\ddot{x}$ are the nodal displacement, velocity, and acceleration vectors.

Assuming that $\dot{x} \approx \dot{x}_{n-1/2}$, Equation (12) was solved with a numerical integration of acceleration $\ddot{x}_n$:

$$\ddot{x}_n = M^{-1}(F_n^{ext} - C\dot{x}_{n-1/2} - F_n^{\text{int}}) \tag{13}$$

Implementation of the central difference equations for velocity and displacement yielded the following relations:

$$\ddot{x}_n = \frac{1}{\Delta t_n}(\dot{x}_{n+1/2} - \dot{x}_{n-1/2}) \Rightarrow \dot{x}_{n+1/2} = \dot{x}_{n-1/2} + \Delta t_n \ddot{x}_n \tag{14}$$

$$\dot{x}_{n+1/2} = \frac{1}{\Delta t_{n+1/2}}(x_{n+1} - x_n) \Rightarrow x_{n+1} = x_n + \Delta t_{n+1/2}\dot{x}_{n+1/2} \tag{15}$$

The main disadvantage of this method is that it is conditionally stable and requires a time step to be limited according to the Courant–Friedrichs–Lewy (CFL) stability condition:

$$\Delta t = \frac{L_E}{Q + \sqrt{Q^2 + c^2}} \tag{16}$$

where Q is a function of the viscous coefficients. C_0 and C_1 is formulated as follows:

$$Q = \begin{cases} C_1 c + C_0 L_E \left|\dot{\varepsilon}_{kk}\right| & \text{for } \dot{\varepsilon}_{\text{kk}} < 0 \\ 0 & \text{for } \dot{\varepsilon}_{\text{kk}} \geq 0 \end{cases} \tag{17}$$

where $L_E = V_E / A_{E\max}$ is the characteristic length of the element; V_E is the volume of the element; $A_{E\max}$ is the largest side of the element area; and c is the adiabatic speed of sound.

4.1.2. ALE Method

The ALE algorithm combines the advantages of the Lagrangian algorithm and the Euler algorithm. The grid is not completely fixed on the medium like the Lagrangian algorithm, nor is it completely fixed in space like the Euler algorithm. The mesh of the ALE algorithm can move freely. The ALE algorithm allows explosives, rocks, and air to freely shuttle between each other. The process of the explosion can be analyzed through the flow of substances. It can directly simulate the detonation process of explosives. It can effectively avoid the problem of calculation interruption caused by excessive mesh deformation in calculations [27].

The core algorithm of the ALE calculation process is the convection algorithm. It is a mapping relationship that controls the material transfer between the new and old grids. When the mesh unit reaches a certain amount of deformation, it needs to be self-repurchased using a certain smoothing algorithm. This article adopts a half index shift algorithm and donor–cell algorithm. Assuming the name of the substance to be transferred in the convection algorithm is f, the amount of transportation required can be calculated using the donor–cell algorithm

$$f_j^{\varphi} = \frac{a_j}{2}(\varphi_{j+\frac{1}{2}}^n + \varphi_{j-\frac{1}{2}}^n) + \frac{|a_j|}{2}(\varphi_{j+\frac{1}{2}}^n + \varphi_{j-\frac{1}{2}}^n) \tag{18}$$

where j is the number of points in which section ($j = 1, 2, 3 \cdots$); n is the number of iterations of the algorithm; a_j is the speed of two discontinuous contacts; $\varphi_{j+\frac{1}{2}}^n$ and $\varphi_{j-\frac{1}{2}}^n$ are the values on both sides of node j at the beginning of the n transportation. It can be expressed as:

$$\varphi_{j+\frac{1}{2}}^{n+1} = \varphi_{j+\frac{1}{2}}^n + \frac{\Delta t}{\Delta x}(f_j^{\varphi} - f_{j+1}^{\varphi}) \tag{19}$$

where Δt is the time step size and Δx is the unit feature length. If it is necessary to solve the three-dimensional flow rate, then it is necessary to use a first-order accuracy half index shift algorithm.

$$\begin{bmatrix} f_{1,j+\frac{1}{2}}^- \\ f_{2,j+\frac{1}{2}}^- \end{bmatrix} = \begin{bmatrix} a & b \\ c & d \end{bmatrix} \begin{bmatrix} \varphi_j^- \\ \varphi_{j+1}^- \end{bmatrix} \tag{20}$$

$$\begin{bmatrix} \varphi_j^+ \\ \varphi_{j+1}^+ \end{bmatrix} = \frac{1}{ad - bc} \begin{bmatrix} d & -b \\ -c & a \end{bmatrix} \begin{bmatrix} f_{1,j+\frac{1}{2}}^- \\ f_{2,j+\frac{1}{2}}^- \end{bmatrix} \tag{21}$$

where a, b, c, and d are matrix constants; f is the name of the substance that needs to be transported; φ is the initial quantity of a certain node; and j is the number of nodes.

4.2. Numerical Simulation Model

4.2.1. Numerical Model

When carrying out numerical simulations, according to the scale and size of on-site bench blasting, a numerical model is established and appropriately simplified to shorten the calculation time. The simplified model is presented in Figure 9. The length, width, and height of the block were 700 cm, 300 cm, and 400 cm, respectively. The blast hole was 100 mm in diameter. Also, nonreflective boundary conditions were adopted at the left, right, bottom, and rear edges of the model, with free boundary conditions (reflective boundaries) considered for the remaining boundaries. The model was then meshed, considering all these inputs and specifications. For rock materials, the Lagrangian mesh method was used, while the Eulerian mesh method was used for explosives and the air. The model mesh grid is shown in Figure 10. The total number of unit divisions in the mesh was 770520, including the rock, explosive, and air units, with nodes shared by the air and explosive units. By defining the keyword *CONSTRAINED_ LAGRANGE_ IN_ SOLID [28], fluid–

solid coupling was achieved for the explosives, air, and rocks. The cm–g–us unit system was adopted in the whole modeling process.

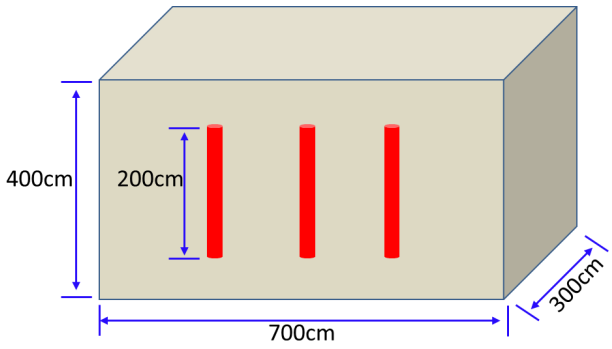


Figure 9. Schematic diagram of the numerical model.

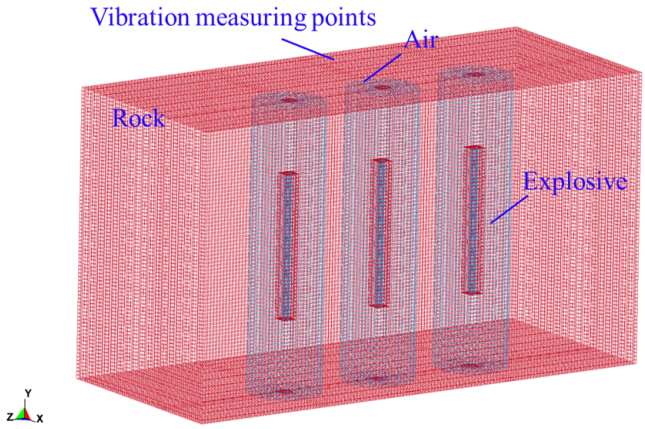


Figure 10. Model grid division.

4.2.2. Material Model

Rock Material Model

The Riedel–Heirmaier–Thomas (RHT) model is a tension compression damage constitutive model proposed by Riedel, Thomas, and Hiermaier based on the traditional Holmquist–Johnson–Cook constitutive model [29]. The model introduces three limit surfaces: the elastic limit surface, the failure surface, and the residual strength surface. On this basis, it can better reflect the dynamic mechanical behavior, strain rate sensitivity, strain hardening, and damage softening characteristics of rocks under different stress states. Overall, the RHT constitutive model is widely used in numerical simulations of explosive shocks and other related fields. In this paper, the numerical simulation of the rock material models employed the * MAT_ RHT model. The material parameters of the rock model were obtained through physical and mechanical tests, references, and SHPB shock tests.

A series of physical and mechanical tests were conducted on sandstone from the Xinguang Open-pit Mine. The density of sandstone is 2440 kg/m^3. The uniaxial compressive strength was 104 MPa. The elastic shear modulus was 16.94 GPa. The uniaxial tensile strength was 10.0 MPa. According to reference [30], the strain rate, failure surface, and damage parameters in the constitutive model have been determined.

Through parameter sensitivity analysis, it was found that the tensile yield surface parameters g_c^* and g_t^*, failure surface parameters A_f and n_f, and shear compression strength ratio f_s^* have a significant impact on the numerical results. Based on the simulation results, these parameters have been adjusted and optimized. The parameters that are not sensitive to simulation results were taken from the values given by Borrvall et al. [31].

The remaining parameters that were difficult to determine were calibrated using SHPB shock tests. The sandstone samples were taken from the Xinguang Open-pit Mine. After polishing, the diameter of the sample was 50 mm, and the height was 25 mm. The SHPB test apparatus is shown in Figure 11. Among them, the length of the bullet was 30 cm. The length of the incident rod was 240 cm. The length of the transmission rod was 140 cm. The bullets and all rods were made of high-strength alloy steel. Its density is 7900 kg/m^3. The wave speed was 5172 m/s. The elastic modulus was 210 GPa. The reasonable range of projectile velocity was determined by the pre-impact velocity, and the final test projectile velocity was 15.61 m/s.

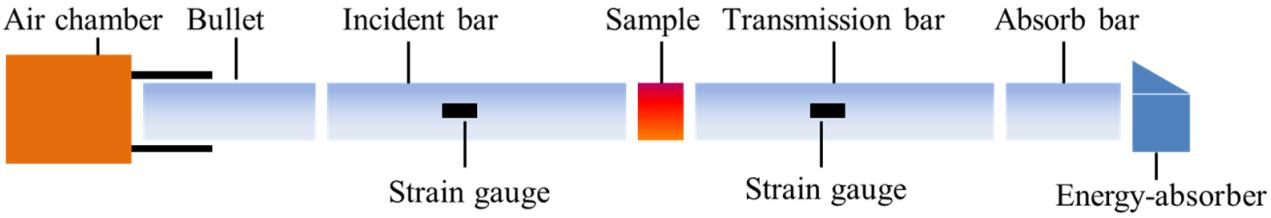


Figure 11. SHPB testing device.

Based on the actual dimensions of the incident rod, transmission rod, and specimen of the SHPB testing system, the model was established in a 1:1 ratio. The rigid rod adopted the elastic constitutive law, and the specimen adopted the RHT constitutive law. After repeated trial and error, we selected a set of parameters that highly matched the simulation results with the experimental data, as shown in Table 2.

Table 2. The parameters of the RHT constitutive model.

Parameter	Value	Parameter	Value	Parameter	Value	Parameter	Value
ρ_0	2.44×10^{-6} kg/mm^3	B_1	0.9	Q_0	0.6805	g_t^*	0.75
P_{el}	0.035 GPa	T_1	22.5 GPa	B	0.0105	ξ	0.5
P_{comp}	0.6 GPa	T_2	0 GPa	β_c	0.012	D_1	0.04
N	3.0	f_c	0.104 GPa	β_t	0.016	D_2	1
α_0	1.164	f_t^*	0.1	$\dot{\varepsilon}_0^c$	3.0×10^{-8} m/s	ε_p^m	0.01
A_1	22.5 GPa	f_s^*	0.2	$\dot{\varepsilon}_0^t$	3.0×10^{-9} m/s	A_f	1.6
A_2	20.25 GPa	G	16.94 GPa	$\dot{\varepsilon}^c$	3×10^{22} m/s	n_f	0.61
A_3	2.1 GPa	A	1.92	$\dot{\varepsilon}^t$	3×10^{22} m/s		
B_0	0.9	n	0.76	g_c^*	0.53		

The comparison between the stress–strain curve obtained from the numerical simulation and experimental results is shown in Figure 12. From the graph, it can be seen that the peak stress and strain of both were almost the same. Under dynamic impact loads, the specimen fractures into numerous fragments. It was relatively close to the results of the experiment, as shown in Figure 13.

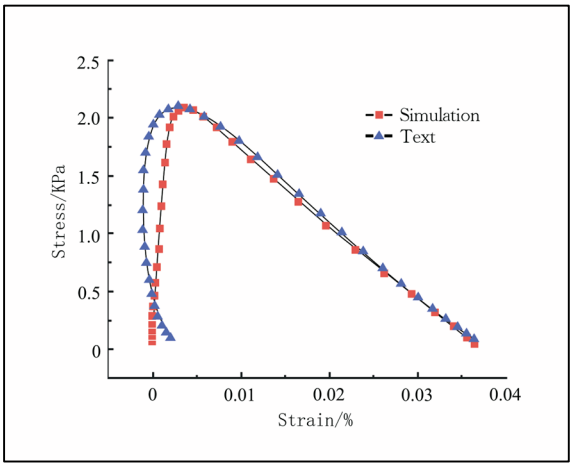
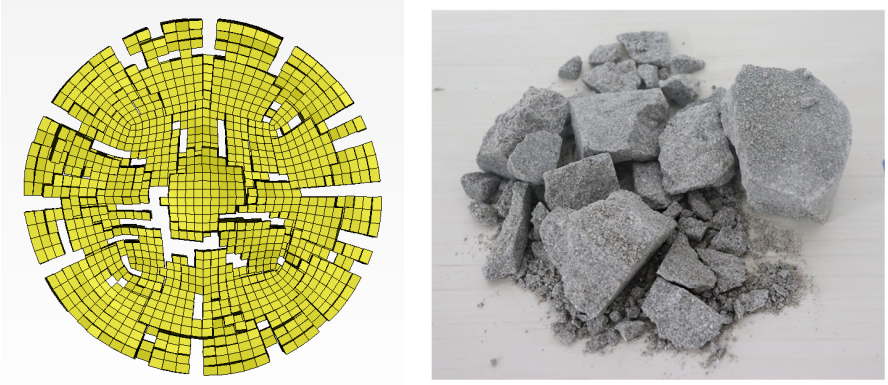


Figure 12. Stress–strain curve of the samples.



(**a**) Numerical simulation results (**b**) test result

Figure 13. Comparison of failure mode of sample.

Explosive Material Model

One of the main advantages of the high-energy explosive materials found in the LS-DYNA material library is that the physical and chemical properties of the explosives can be accurately described. Regarding the pressure arising in the unit of high explosives after initiation, it was obtained using the Jones–Wilkins–Lee (JWL) equation of state [32]. Since the equation of state is a semi-empirical equation with no chemical reaction, utilizing parameters determined using empirical methods, the expansion-driven work process of the detonation products can be described more accurately, as shown in Equation (22).

$$P = A(1 - \frac{\omega}{R_1 V})e^{R_1 V} + B(1 - \frac{\omega}{R_2 V})e^{R_2 V} + \frac{\omega E}{V} \quad (22)$$

where A, B, R_1, R_2, ω: Undetermined constants

E: Internal energy of detonation products per unit volume;
V: The relative volume of detonation products, i.e., the ratio of detonation product volume to the initial volume.

Regarding the explosive material model, the material model 008 in LS-DYNA was adopted, namely the * MAT_ HIGH_ EXPLOSIVE_ BURN model. In addition, the equation of the state of the explosives was defined as * EOS_ JWL. The 2# rock emulsion explosives were used to conduct numerical simulations. The parameters of the explosives were obtained through experiments. The density of the explosives was 1.08 g/cm^3. The detonation speed was 3800 m/s, and the detonation pressure was 9.9 GPa. For other parameters, refer to reference [33]. The parameters are listed in Table 3.

Table 3. The parameters of the explosive material model.

Density ρ/g·cm^{-3}	Detonation Velocity/cm·μs^{-1}	Explosion Pressure *Pcj*/GPa	*A*/GPa	*B*/GPa	R_1	R_2	ω	*E*/GPa
1.08	0.380	9.9	214.4	182	4.2	0.9	0.15	4.19

Air Material Model

In this paper, an empty material constitutive model was used for air simulation, namely the * MAT_ NULL model. Meanwhile, the state equation adopts a Linear_ Polynomial as follows:

$$p = C_0 + C_1\mu + C_2\mu^2 + C_3\mu^3 + (C_4 + C_5\mu + C_6\mu^2)E \quad (23)$$

$$\mu = \frac{1}{V} - 1E_0V_0 \quad (24)$$

where C_0, C_1, C_2, C_3, C_4, C_5, C_6 is a user-defined constant, p is pressure, and E is the initial internal energy per unit.

The density of air is considered as 1.29 kg/m^3 in the calculation, and the parameters of the state equation are from reference [34] as shown in Table 4.

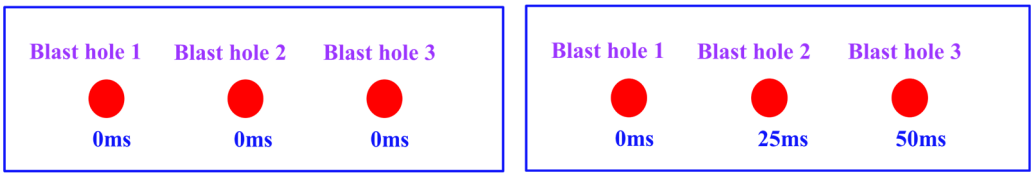
Table 4. Air state equation parameters.

C_0	C_1	C_2	C_3	C_4	C_5	C_6	E_0	V_0
0.0	0.0	0.0	0.0	0.4	0.4	0.0	2.5×10^{-6}	-

4.3. Ways of Blasting

To better analyze the blasting effect of the three-hole simultaneous blasting method, this study divided the numerical simulation process into two scenarios: one scenario represented the three-hole simultaneous blasting method, and the other represented the hole-by-hole blasting method.

The three-hole simultaneous blasting method had no delay time between the holes. On the other hand, the hole-by-hole blasting method detonated three holes sequentially from left to right, with a delay time of 25 ms between holes. This set time was consistent with the delay time adopted between the onsite test sections. The delay time setting of the numerical simulation borehole is shown in Figure 14.



(**a**) Three-hole simultaneous blasting (**b**) Hole-by-hole blasting

Figure 14. Delay time setting for numerical simulations.

4.4. Simulation Calculation and Analysis

4.4.1. Reliability Analysis of Numerical Simulation Results

To verify the reliability of the numerical simulation results, a unit of the numerical model was selected for investigation. The considered unit was located at a certain distance directly behind the borehole, as depicted in Figure 10. In this investigation, the value of the vibration velocity of this unit is extracted. By comparing the vibration data monitored at similar locations to the onsite blasting test results, as shown in Figure 15, the reliability of numerical simulations was analyzed.

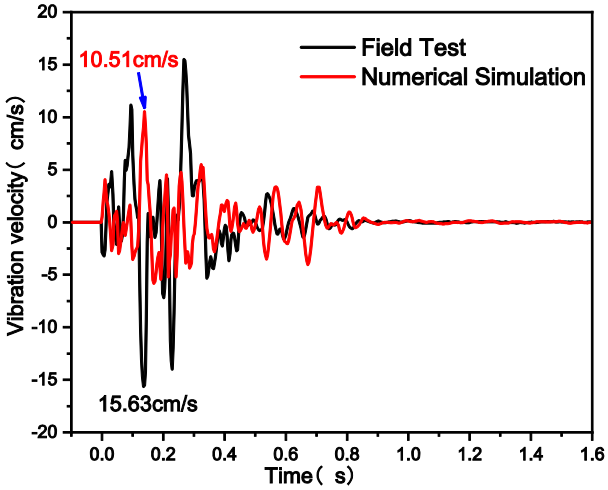
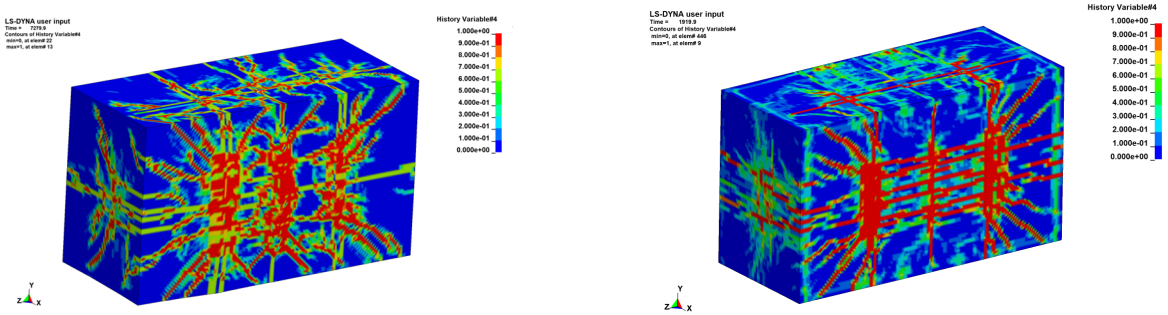


Figure 15. Comparison of the vibration velocity between numerical simulations and onsite test data.

As shown in Figure 15, it was noted that there were multiple peak values of surface vibration velocity caused by the onsite blasting tests. These were related to the blasting method of the onsite blast holes. During the onsite blasting, multiple segments of blast holes were sequentially initiated. Considering the numerical simulation results, it was noted that there was only one vibration velocity peak of 10.51 cm/s for the three-hole simultaneous blasting, whereas the peak surface vibration velocity caused by the onsite blasting tests was 15.63 cm/s. On this basis, it was shown that the peak vibration velocities generated by the onsite blasting tests and numerical simulations were of the same order of magnitude. At the same time, the blasting vibration velocities generated by both the onsite blasting tests and numerical simulations ultimately decayed to 0 cm/s over time. Based on these findings, it was highlighted that the different material models and parameters selected in the numerical simulation process were feasible. As a result, it can be claimed that the simulation results of the three-hole simultaneous blasting method and the hole-by-hole blasting were reliable, considering the established model.

4.4.2. Numerical Simulation Results

During the blasting process, the stress waves propagated outward. In the process of numerical simulation, the severity of the damage caused by the explosion can be observed through a dynamic blasting process simulated by the model. Figure 16 shows the damage caused by the hole-by-hole blasting and the three-hole simultaneous blasting.



(**a**) Model damage by the hole-by-hole blasting method (**b**) Model damage by three-hole simultaneous blasting method

Figure 16. Numerical model damage.

As shown in Figure 16a, the severity level of the damage caused at the front of the blast hole was relatively high when the hole-by-hole blasting method was adopted, with a spider-like crack observed around each blast hole. In addition, the damage severity level

at the bottom of the blast hole was relatively high, resulting in a local unevenness at the bottom of the model and establishing a root. Meanwhile, there was also a certain degree of damage caused to the model at the front and rear sides, resulting in a non-smooth interface throughout the latter half of the model.

Furthermore, Figure 16b highlights that a transverse crack developed in the direction of the connection line at the center of the blast hole when the three-hole simultaneous blasting method was adopted. On the other hand, the severity level of the damage caused to the model at the bottom of the blast hole was relatively low.

4.4.3. Stress Analysis at Typical Locations

To better analyze the outcomes of the fragmentation as produced by the model when the hole-by-hole blasting method and the three-hole simultaneous blasting method were used, a total of 10 measurement points were placed at typical positions along the model. In addition, five testing points were placed in front of the two holes and on the front side of the blast hole, as shown in Figure 17.

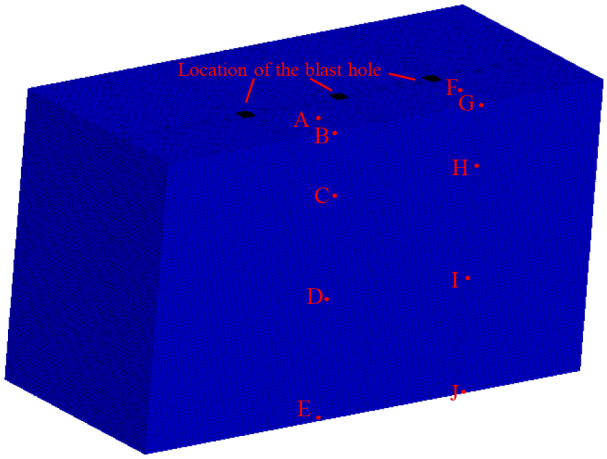


Figure 17. Typical measurement points of the model.

Employing the Ls-PrePost (4.3) post-processing software, the maximum effective stress applied at these 10 typical measurement points in the model was determined and recorded. The results are summarized in Table 5.

Table 5. Maximum effective stress at the typical locations of the model (Unit: GPa).

Measurement Point	In Front of the Middle Part of the Two Blast Holes					Front Side of the Blast Hole				
	A	**B**	**C**	**D**	**E**	**F**	**G**	**H**	**I**	**J**
Hole-by-hole blasting	41.9	47.0	35.4	48.5	43.5	45.2	13.1	18.1	5.35	15.5
Three-hole simultaneous blasting	43.5	42.1	44.9	54.3	19.8	41.7	38.4	53.5	67.9	26.9

The data presented in Table 4 was processed using the Origin (8.0) which is professional data processing software. As a result, Figure 18 shows the maximum effective stress histogram at each measurement point when the hole-by-hole blasting method and the three-hole simultaneous blasting method were applied, respectively.

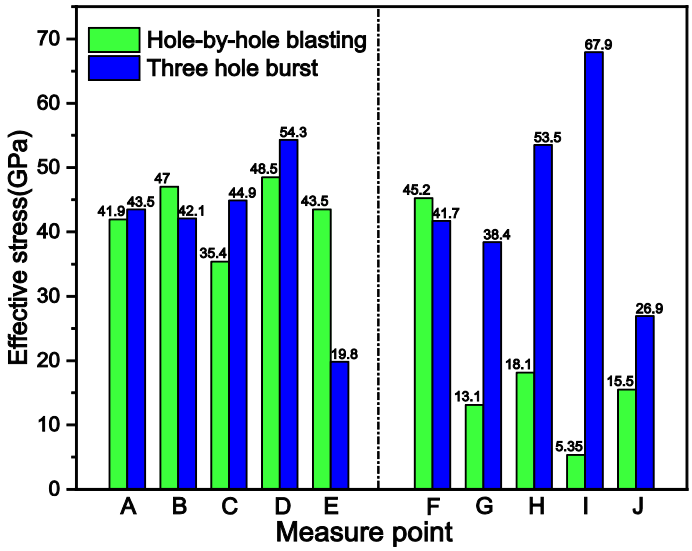


Figure 18. Histogram of maximum effective stress at the measurement points of the model.

It was noted from the results presented in Figure 18 that when the hole-by-hole blasting method was used, the effective stress at the measurement points B, C, and F was relatively high, reaching 47 GPa, 48.5 GPa, and 45.2 GPa, respectively. On the other hand, when the three-hole simultaneous blasting method was adopted, the effective stress at the measurement points D and I was found to be relatively high, attaining 54.3 GPa and 67.9 GPa, respectively. Overall, the effective stress was highlighted as being relatively high at the measurement point deployed in the front side of the blast hole when the three-hole simultaneous blasting method was employed.

4.4.4. Characteristics of Displacement Changes at Typical Locations

In this section, the Ls-PrePost (4.3) post-processing software was applied to determine and record the maximum displacement at the ten typical measurement points selected in the model. The results are presented in Table 6.

Table 6. The maximum displacement at typical locations of the model (unit: cm).

Measurement Point	In Front of the Middle Part of the Two Blast Holes					Directly ahead of the Blast Hole				
	A	B	C	D	E	F	G	H	I	J
Hole-by-hole blasting	3.88	5.02	6.47	9.49	5.05	7.28	8.66	15.8	21.2	9.01
Three-hole simultaneous blasting	5.06	10.7	18.3	24.1	10.8	5.94	10.6	17.8	31.9	10.8

Furthermore, the data shown in Table 5 was processed using the Origin professional data processing software. On this basis, Figure 19 presents the histogram of the maximum displacement at each measurement point as drawn when the hole-by-hole blasting and three-hole simultaneous blasting methods were adopted.

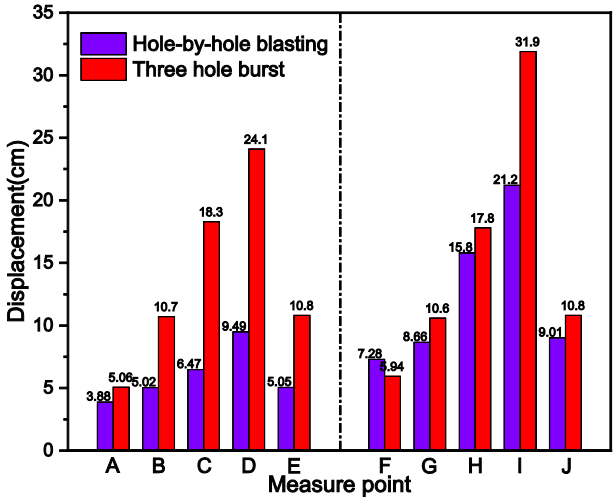


Figure 19. Histogram of maximum displacement at the measurement points of the model.

According to the results presented in Figure 19, the displacement at the measurement points D, H, and I was relatively significant when the hole-by-hole blasting method was used, reaching 9.48 cm, 15.8 cm, and 21.2 cm, respectively. On the other hand, when implementing the three-hole simultaneous blasting method, the displacement at the measurement points C, D, and I was found to be relatively significant, attaining 18.3 cm, 24.1 cm, and 31.9 cm, respectively. Overall, the displacement at each measurement point was much more significant when the three-hole simultaneous blasting method was applied compared to the case when the hole-by-hole blasting method was adopted.

5. Results and Discussion

Based on actual engineering practice and theoretical analysis, this study proposed a method of three-hole simultaneous blasting for open-pit mine bench blasting and conducted onsite blasting experiments. The onsite blasting tests highlighted that the three-hole simultaneous blasting approach could effectively overcome the problem of rear row strain in the blasting area. At the same time, the obtained blasting piles were relatively concentrated, with a uniform size and no large blocks generated. To further analyze the advantages of the three-hole simultaneous blasting method and to examine the evolution process of rock fractures, a comparative analysis was conducted for the three-hole simultaneous blasting and the hole-by-hole blasting, employing numerical simulations. It was found that under the three-hole simultaneous blasting method, obvious damage was reported in the form of macroscopic cracks, formed in the direction of the connection line at the center of the blast hole. This was because the shock wave generated by the explosion met between two blast holes. In addition, the rock on the connection line was subjected to compressive stress, resulting in vertical tensile stress. Generally, the tensile strength of rocks was much smaller than the compressive strength, and cracks occurred along the connection between the two holes. This finding was consistent with the principle of smooth blasting studied by many researchers in the literature [35]. At the same time, compared to the hole-by-hole blasting method, the effective stress and displacement generated in front of the blast hole were relatively large under the three-hole simultaneous blasting method. In this case, a maximum effective stress of 67.9 GPa and a maximum displacement of 31.9 cm were reported. This was because the single-stage charge amount of the three-hole simultaneous blasting was three times that of the hole-by-hole blasting, improving the blasting power significantly.

This paper presented a three-hole simultaneous blasting technology that combined the stepwise blasting technology and the smooth blasting theory. The proposed approach yielded more advantages in terms of the blasting effect [19,36]. To the best of the authors' knowledge, this is the first time this technology has been proposed, and there have been

no similar reports in the relevant literature. In this regard, this technology is of great significance and provides a reference for similar mine bench blasting.

However, the mechanism of rock fragmentation by blasting is complex. Next, it is necessary to further strengthen the on-site testing and numerical simulation research of the three-hole step-by-step detonation technology in different mines.

6. Conclusions

Aiming to address the actual problem of the rear row original rock strain, this paper proposed a three-hole simultaneous blasting technology. The feasibility of the technology was verified through onsite blasting experiments and numerical simulations. Based on the obtained results, the following conclusions are drawn:

(1) Through onsite blasting tests, it was found that the three-hole simultaneous blasting technology yielded a good blasting effect, with fewer flying stones and more concentrated blasting piles. Additionally, the original rock in the rear row had no obvious tensile damage, and the block size was relatively uniform, with no large blocks produced.

(2) Numerical simulations concluded that compared to the hole-by-hole blasting method, the three-hole simultaneous blasting method provided more advantages. A transverse crack formed in the direction of the connection line at the center of the blast hole. This was consistent with the findings of the onsite blasting experiments.

(3) The three-hole simultaneous blasting technology proposed in this paper combined the stepwise blasting technology and the smooth blasting theory. It could effectively avoid the problem of rear row strain in the blasting area. Based on the preliminary results reported in this work, the proposed technology could be promoted and applied to similar mining bench blasting.

(4) In the future, it is necessary to further strengthen the on-site testing and numerical simulation research of the three-hole step-by-step detonation technology in different mines.

Author Contributions: Conceptualization, X.Z. and Z.L.; Methodology, X.Z. and Z.L.; Validation, W.G.; Formal analysis, X.Z. and Z.W.; Investigation, X.Z., Z.W. and W.G.; Resources, Z.L.; Data curation, Z.L.; Writing—original draft, X.Z., Z.W. and W.G.; Writing—review & editing, X.Z. and Z.L.; Visualization, Z.W. and W.G.; Supervision, X.Z. and Z.L. All authors have read and agreed to the published version of the manuscript.

Funding: This work is supported by the Beijing Postdoctoral Research Foundation (2022-ZZ-100), the Chaoyang District Postdoctoral Work Foundation, and the Foundation of Hubei Key Laboratory of Blasting Engineering.

Institutional Review Board Statement: Not applicable.

Informed Consent Statement: Not applicable.

Data Availability Statement: Data are contained within the article.

Conflicts of Interest: Author Zheng Wei was employed by the company Inner Mongolia Kinergy Blasting Co., Ltd. The remaining authors declare that the research was conducted in the absence of any commercial or financial relationships that could be construed as a potential conflict of interest.

References

1. Chen, Y.; Li, C.; Wang, W.; Liu, H.; Yao, Y.; Ni, S.; Sarajpoor, S. Study on the liquefaction characteristics of saturated sands by millisecond delay blasting. *Soil Dyn. Earthq. Eng.* **2023**, *164*, 107584. [CrossRef]
2. Ma, J.; Li, X.; Wang, J.; Li, Q.; Zuo, T.; Wu, X.; Hou, M. Numerical Simulation on Selection of Optimal Delay Time for Precise Delay Blasting. *Shock. Vib.* **2021**, *2021*, 4593221. [CrossRef]
3. Bikarregi, A.; Dominguez, S.; Brizuela, M.; López, A.; Suarez-Vega, A.; Agustín-Sáenz, C.; Presa, M.; López, G.A. Direct Fabrication of a Copper RTD over a Ceramic-Coated Stainless-Steel Tube by Combination of Magnetron Sputtering and Sol-Gel Techniques. *Sensors* **2023**, *23*, 5442. [CrossRef]

4. Liu, R.Y.; Luo, S.X.L.; Hirst, E.S.; Doona, C.J.; Swager, T.M. Bifunctional diazirine reagent for covalent dyeing of Kevlar and inert polymer materials. *Polym. Chem.* **2023**, *14*, 4205–4215. [CrossRef]
5. Murphy, L.A.; Winters, A.C. Emerging and Future Targeted Therapies for Pediatric Acute Myeloid Leukemia: Targeting the Leukemia Stem Cells. *Biomedicines* **2023**, *11*, 3248. [CrossRef]
6. Cui, J.; Xie, L.; Qin, Y.; Liu, X.; Wang, J.; Qian, J. Cracks propagation characteristics of double-hole delay blasting in soft-hard composite rock mass. *Sci. Rep.* **2023**, *13*, 8762. [CrossRef] [PubMed]
7. Qiu, X.; Hao, Y.; Shi, X.; Hao, H.; Zhang, S.; Gou, Y. Numerical simulation of stress wave interaction in short-delay blasting with a single free surface. *PLoS ONE* **2018**, *13*, e0204166. [CrossRef] [PubMed]
8. Tang, H.-L.; Liu, X.; Yang, J.; Yu, Q. Experimental Study on the Influence of Delay Time on Rock Fragmentation in Bench Blasting. *Appl. Sci.* **2023**, *13*, 85. [CrossRef]
9. Zhang, P.; Bai, R.; Sun, X.; Li, H.; Fei, H.; Bao, S. A Study of Millisecond Blasting on High Bench at Barun Iron Ore Operation. *Geofluids* **2021**, *2021*, 3645438. [CrossRef]
10. Hosseini, M.; Khandelwal, M.; Lotfi, R.; Eslahi, M. Sensitivity analysis on blast design parameters to improve bench blasting outcomes using the Taguchi method. *Geomech. Geophys. Geo-Energ. Geo-Resour.* **2023**, *9*, 9. [CrossRef]
11. Dzimunya, N.; Besa, B.; Nyirenda, R. Prediction of ground vibrations induced by bench blasting using the random forest algorithm. *J. South. Afr. Inst. Min. Metall.* **2023**, *123*, 123–132. [CrossRef]
12. Lv, S.; Yao, H.; Wang, L. Research on the Application of Electronic Digital Detonator in Iron Mine Blasting. *Eng. Blasting* **2013**, *19*, 53–56. (In Chinese)
13. Cheng, G.; Zhang, Q.; Tang, C.; Wang, Y.; Cheng, S.; Jiang, W. The application of digital electronic detonators in high slope blasting excavation. *Chem. Miner. Process.* **2018**, *47*, 52–55. (In Chinese)
14. He, Z.; Liu, J. The application of digital electronic detonators in underwater reef blasting. *Eng. Blasting* **2017**, *23*, 77–81. (In Chinese)
15. Chen, Y.; Wang, P.; Chen, J.; Zhou, M.; Yang, H.; Li, J. Calculation of blast hole charge amount based on three-dimensional solid model of blasting rock mass. *Sci. Rep.* **2022**, *12*, 541. [CrossRef]
16. Hosseini, S.; Pourmirzaee, R.; Armaghani, D.J.; Sabri, M.M.S. Prediction of ground vibration due to mine blasting in a surface lead–zinc mine using machine learning ensemble techniques. *Sci. Rep.* **2023**, *13*, 6591. [CrossRef]
17. Ding, W.J. A Transformer-Based Framework for Misfire Detection from Blasting-Induced Ground Vibration Signal. *IEEE Sens. J.* **2022**, *22*, 18698–18708. [CrossRef]
18. Gao, J.; Cheng, P.; Ren, J.J.; Wang, F.N. Experimental Study on Frequency Modulation Damping Effect of Digital Detonator in Road Clearance Blasting. *Shock. Vib.* **2023**, *2023*, 4645101. [CrossRef]
19. Ma, J.; Li, X.; Wang, J.; Tao, Z.; Zuo, T.; Li, Q.; Zhang, X. Experimental Study on Vibration Reduction Technology of Hole-by-Hole Presplitting Blasting. *Geofluids* **2021**, *2021*, 5403969. [CrossRef]
20. Shi, J.J.; Miao, X.P.; Meng, H.L.; An, H.M.; Zhang, W. Study on Critical Damage Width of Parallel Double-Free Surface Blasting. *Front. Earth Sci.* **2022**, *10*, 884558. [CrossRef]
21. Wang, M.L.; Li, X.S.; Li, Q.H.; Hu, Y.J.; Chen, Q.S.; Jiang, S. Study on Blasting Technology for Open-Pit Layering of Complex Mine Adjacent to High and Steep Slope. *Front. Earth Sci.* **2021**, *9*, 773872. [CrossRef]
22. Nourian, A.; Moomivand, H. Development of a New Model to Predict Uniformity Index of Fragment Size Distribution Based on the Blasthole Parameters and Blastability Index. *J. Min. Sci.* **2020**, *56*, 47–58. [CrossRef]
23. Liu, X.; Wang, G.; Liu, T.; Lin, M.; Lei, H.; Mandal, A.K. Study on dynamic mechanical properties of phosphate rock through experimental tests and mesoscale simulation. *Arab. J. Geosci.* **2020**, *13*, 969. [CrossRef]
24. Baranowski, P.; Damaziak, K.; Mazurkiewicz, Ł.; Mertuszka, P.; Pytel, W.; Małachowski, J.; Pałac-Walko, B.; Jones, T. Destress Blasting of Rock Mass: Multiscale Modelling and Simulation. *Shock Vib.* **2019**, *2019*, 2878969. [CrossRef]
25. Pająk, M.; Baranowski, P.; Janiszewski, J.; Kucewicz, M.; Mazurkiewicz, Ł.; Łaźniewska-Piekarczyk, B. Experimental testing and 3D meso-scale numerical simulations of SCC subjected to high compression strain rates. *Constr. Build. Mater.* **2021**, *302*, 124379. [CrossRef]
26. Baranowski, P.; Mazurkiewicz, L.; Małachowski, J.; Pytlik, M. Experimental testing and numerical simulations of blast-induced fracture of dolomite rock. *Meccanica* **2020**, *55*, 2337–2352. [CrossRef]
27. Hallguist, J.O. *LS-DYNA Theory Manual*; Livermore Software Technology Corporation: Livermore, CA, USA, 2006.
28. Hallguist, J.O. *LS-DYNA 970 Keyword User's Manual*; Livermore Software Technology Corporation: Livermore, CA, USA, 2003.
29. Oyejide, A.J.; Awonusi, A.; Ige, E.O. Fluid-structure interaction study of hemodynamics and its biomechanical influence on carotid artery atherosclerotic plaque deposits. *Med. Eng. Phys.* **2023**, *117*, 103998. [CrossRef]
30. Li, S.; Ling, T.; Liu, D.; Liang, S.; Zhang, R.; Huang, B.; Liu, K. Determination of Rock Mass Parameters for the RHT Model Based on the Hoek–Brown Criterion. *Rock Mech. Rock Eng.* **2023**, *56*, 2861–2877. [CrossRef]
31. Borrvall, T.; Riedel, W. The RHT concrete model in LS-DYNA. In Proceedings of the 8th European LS-DYNA Users Conference, Strasbourg, France, 23–24 May 2011.
32. Wang, Y. *Research on Rock Mass Blasting Fragmentation Model Based on RHT Constitutive Theory*; China University of Mining and Technology: Beijing, China, 2015. (In Chinese)
33. Ko, Y.; Shin, C.; Jeong, Y.; Cho, S. Blast Hole Pressure Measurement and a Full-Scale Blasting Experiment in Hard Rock Quarry Mine Using Shock-Reactive Stemming Materials. *Appl. Sci.* **2022**, *12*, 8629. [CrossRef]

34. Li, X.; Liu, K.; Yang, J.; Sha, Y.; Song, R. Numerical study on the effect of in-situ stress on smoothwall blasting in deep tunneling. *Undergr. Space* **2023**, *11*, 96–115.
35. Wang, J.; Cao, A.; Liu, J.; Wang, H.; Liu, X.; Li, H.; Sun, Y.; Long, Y.; Wu, F. Numerical Simulation of Rock Mass Structure Effect on Tunnel Smooth Blasting Quality: A Case Study. *Appl. Sci.* **2021**, *11*, 10761. [CrossRef]
36. Chen, Y.; Chen, S.; Wu, Z.; Dai, B.; Xv, L.; Wu, G. Optimization of Genetic Algorithm through Use of Back Propagation Neural Network in Forecasting Smooth Wall Blasting Parameters. *Mathematics* **2022**, *10*, 1271. [CrossRef]

Disclaimer/Publisher's Note: The statements, opinions and data contained in all publications are solely those of the individual author(s) and contributor(s) and not of MDPI and/or the editor(s). MDPI and/or the editor(s) disclaim responsibility for any injury to people or property resulting from any ideas, methods, instructions or products referred to in the content.